Supplemental Data

Structural Analysis of the Anaphase-Promoting Complex Reveals Multiple Active Sites and Insights into Polyubiquitylation

Lori A. Passmore, Christopher R. Booth, Catherine Vénien-Bryan, Steven J. Ludtke, Céline Fioretto, Louise N. Johnson, Wah Chiu, and David Barford

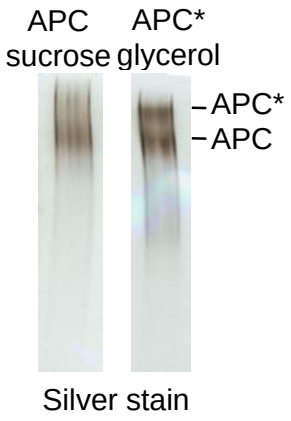

Figure S1 - Purification of monomeric and dimeric APC.

Monomeric APC was purified from a 10-40% sucrose gradient and dimeric APC (APC*) was purified from a 20-60% glycerol gradient. The peak fractions were diluted to 15% sucrose and 20% glycerol respectively, to assist with concentration to 0.136 mg/ml. When the glycerol concentration of dimeric APC was diluted, ~50% of the dimeric APC converted into monomeric APC, suggesting that high glycerol stabilises the dimeric (APC*) form. The concentrated fractions were analysed by non-denaturing PAGE and silver staining.

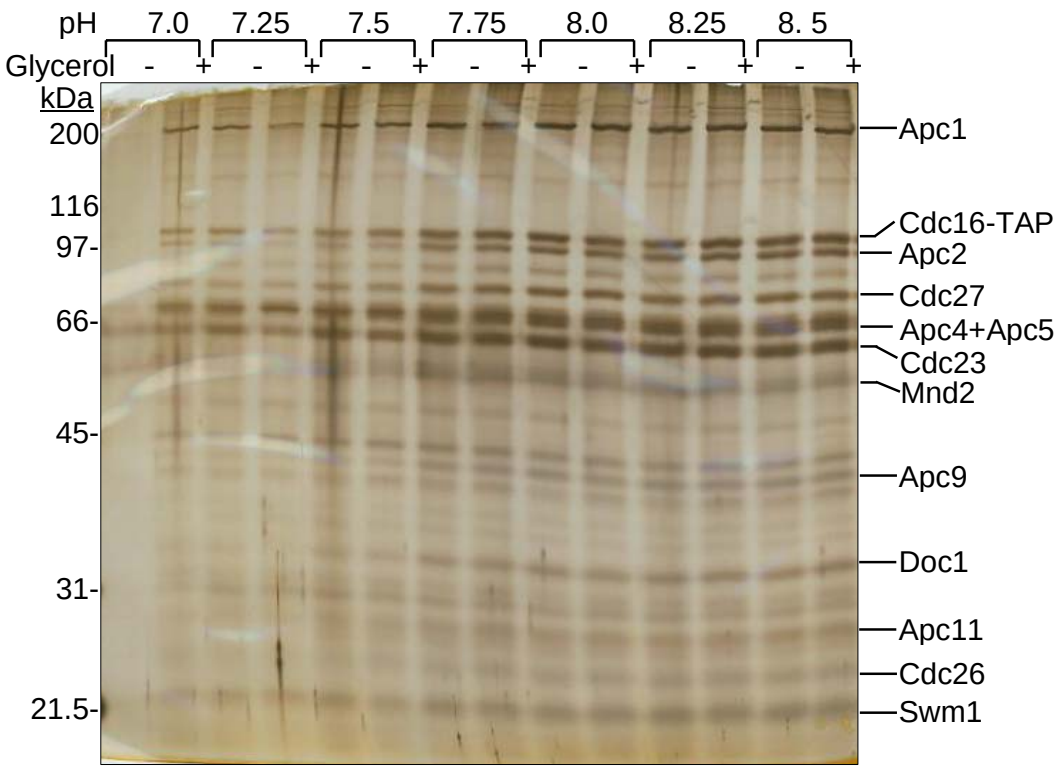

Figure S2 - Examination of APC stability.

The APC is sensitive to pH less than 7.5 since the amount of APC eluted from calmodulin sepharose decreases under these conditions. The stability of APC was determined at seven different pHs, with and without glycerol. APC purified from CDC16-TAP yeast was incubated on 50 µl calmodulin sepharose at 4°C in 10 mM Tris-Cl, 150 mM NaCl, 1 mM magnesium acetate, 3 mM DTT, 2 mM $CaCl_2$ and +/- 5% (w/v) glycerol with pH 7.0, 7.25, 7.5, 7.75, 8.0, 8.25 or 8.5. After three days incubation, the calmodulin sepharose was washed three times with 0.5 ml buffer and the APC was eluted in 0.3 ml elution buffer (10 mM Tris-Cl, 150 mM NaCl, 1 mM magnesium acetate, 3 mM DTT, 2 mM EGTA) with the same pH and glycerol content as the washes. 100 µl of each eluate was run on 8% SDS-PAGE and analysed by silver-staining. Known APC subunits are labelled. Unlabelled bands are likely breakdown products or contaminating proteins.

Since less APC elutes from calmodulin sepharose at pH less than 7.5, low pH may cause the APC to precipitate or dissociate. The APC appears to be stable at pH 8.0. The stability of human APC is also sensitive to low pH since some subunits dissociate from the complex at pH 6.5 (Vodermaier et al., 2003). For cryo-EM, we had prepared APC in Tris buffer, pH 8.0. However, we suspected that the temperature dependence of Tris buffer was problematic for APC stability since brief warming of the specimen during grid preparation would significantly lower the pH. Observations of Tris-buffered APC in vitreous ice are consistent with this notion since many particles appeared to be damaged and aggregated. HEPES buffer, which does not have significant temperature dependence, improved the homogeneity of particles and resulted in more even spreading of the sample on grids (see Figure 4A).

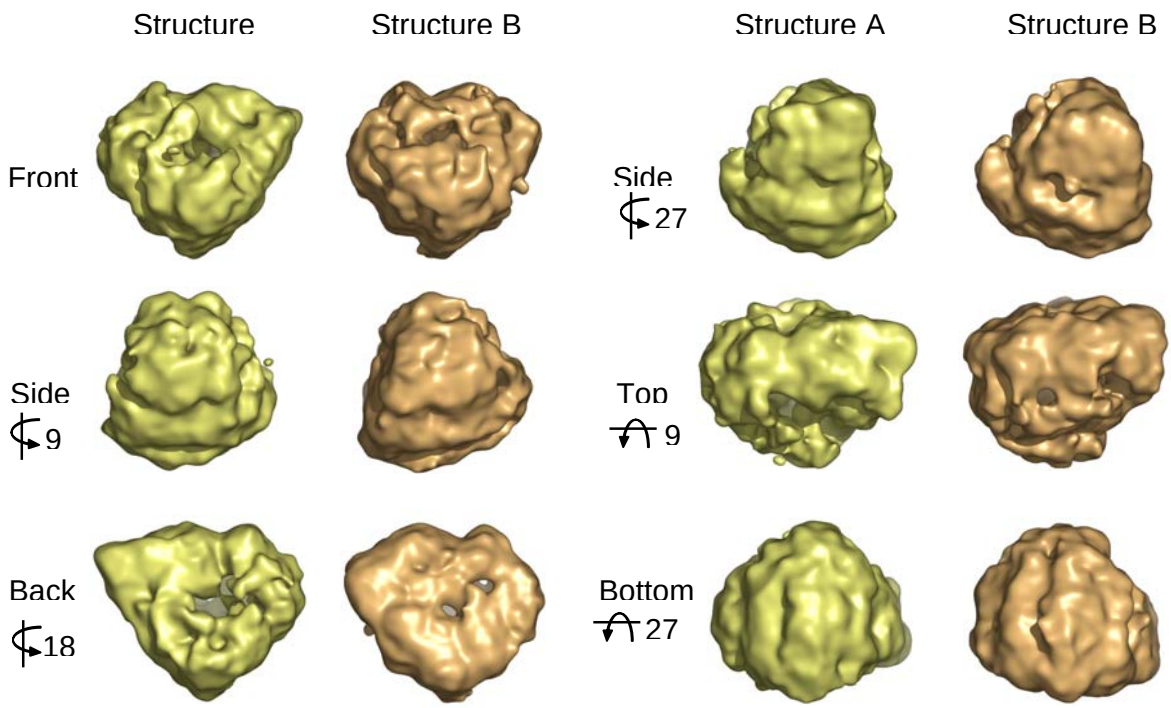

Figure S3 - Heterogeneity of APC.

During initial refinements of the APC structure, we were unable to achieve a resolution higher than ~30 Å. With 19 384 particles, we would expect to have a higher resolution. Thus, we used the *multirefine* command in EMAN to determine if more than one structure was present in our data set. Using this method, the data was partitioned into 2 sets (7500 and 6800 particles) which converged to slightly different structures (structure **A** and structure **B** respectively) each having resolutions of ~20 Å. Although the differences between these two structures are small, data set A routinely gave structure A and data set B routinely gave structure B. Structure A is presented throughout the paper. The positions of helical repeat proteins in Figure 5 also fit well to structure B. Rotations are shown relative to the front view (top left).

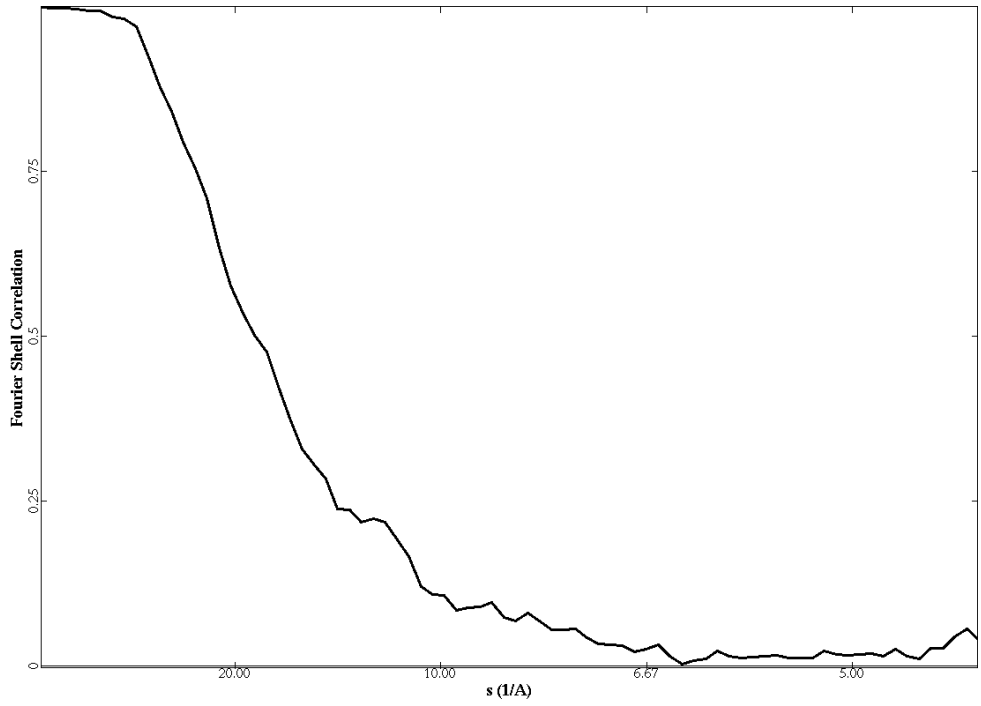

Figure S4: Resolution curve of cryo-EM APC reconstruction (structure A).

The Fourier Shell Correlation (FSC) was calculated between two APC reconstructions (each created from half of the data) and plotted with respect to spatial frequency ($Å^{-1}$). The resolution at 0.5 FSC is ~19 Å (red line).

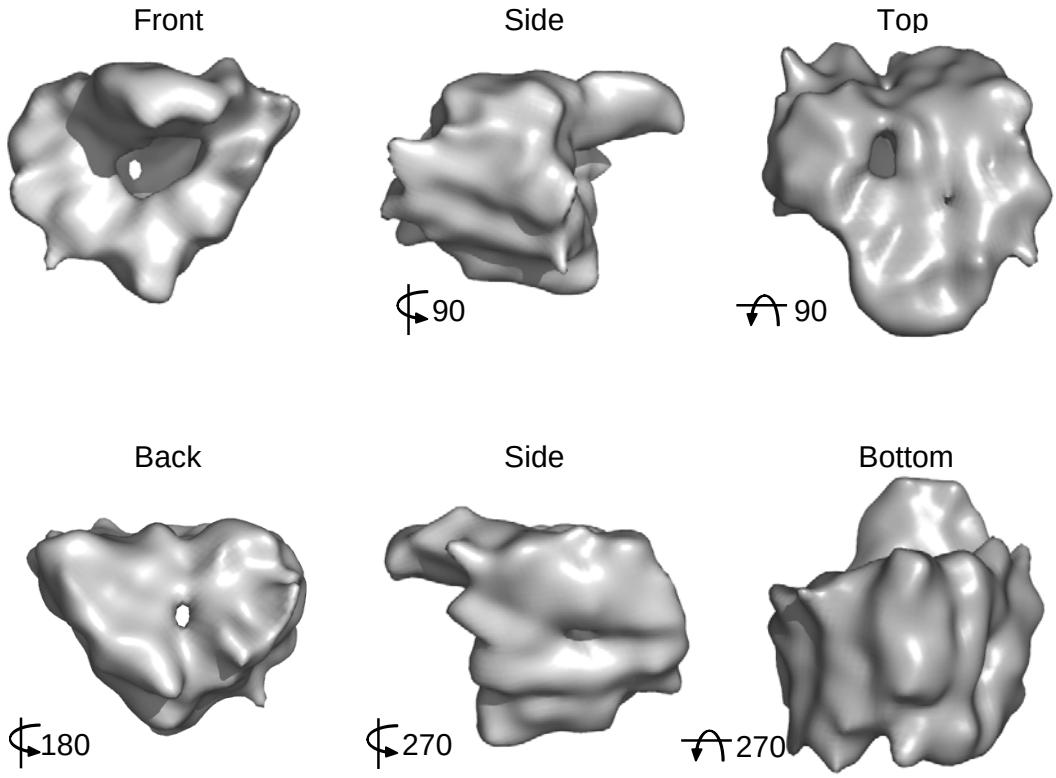

Figure S5: Random Conical Tilt Reconstruction of Negative Stained APC.

For an initial three-dimensional reconstruction of monomeric negative stained APC, we used random conical tilt. 2138 unlabelled particles were simultaneously picked from 25 pairs of tilted (50°) and untilted micrographs. Untilted specimen images were subjected to reference free alignment and sorted into 20 classes. The corresponding tilted images were back-projected and 20 volumes were produced. Eleven of these volumes were aligned in a common orientation in real space and the data were merged (1399 particles) to compute an initial APC model. This model was iteratively refined using projection matching with 5141 particles, then further refined with an additional 1349 gold labelled particles ($APC^{Apc11\text{-}6His}$) (6490 particles total). The resolution of this model is 29 Å at 0.5 FSC and 24 Å at the 3 sigma cutoff. The APC had a preferred orientation on the grid in negative staining (usually with the back face laying on the grid surface). Therefore, the particle appears elongated in one direction (perpendicular to the front/back views). This model was not used as a

starting model for the cryo-EM reconstruction. However, the cryo-EM and negative stain reconstructions, which were determined independently and using different methods, are in good agreement. Namely, the front view shows a triangular shape with a large cavity in the centre and the side views reveal long ridges extending along the length of the particle.

A

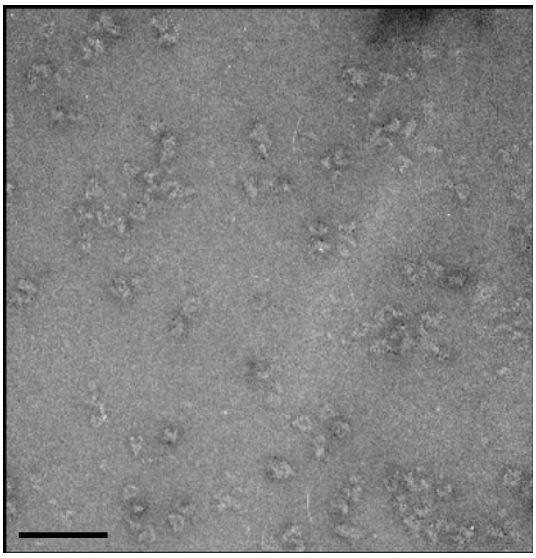

B Apc11-6His

```
MKVKINEVHS VFAWSWHIPS TSDEDAANND PIGNDEDEDV CGICRASYNG  50
TCPSCKFPGD QCPLVIGLCH HNFHDHCIYR WLDTPTSKGL CPMCRQTFQL 100
QKGLAINDAH VQKFVEIVSR RREEMIEEGV AEEFVDFDEP IRQNTDNPIG 150
RQQVDTILDE DFLLRAAGRR IPGGHHHHHH
```

C Cdc23-6His

```
MNDDSQDKII HDIRIQLRKA ATELSRWKLY GSSKWAAEAL AGLAEAIDVD  50
QTHSLADESP LRNKQGVPKQ MFEIPQNGFG LSETEYDLYL LGSTLFDAKE 100
FDRCVFFLKD VTNPYLKFLK LYSKFLSWDK KSQESMENIL TTGKFTDEMY 150
RANKDGDGSG NEDINQSGHQ RANLKMVSNE HESQSNISSI LKEINTFLES 200
YEIKIDDDEA DLGLALLYYL RGVILKQEKN ISKAMSSFLK SLSCYSFNWS 250
CWLELMDCLQ KVDDALLLNN YLYQNFQFKF SENLGSQRTI EFNIMIKFFK 300
LKVFEELNGQ LEDYFEDLEF LLQVFPNFTF LKAYNATISY NNLDYVTAES 350
RFDDIVKQDP YRLNDLETYS NILYVMQKNS KLAYLAQFVS QIDRFRPETC 400
CIIANYYSAR QEHEKSIMYF RRALTLDKKT TNAWTLMGHE FVELSNSHAA 450
IECYRRAVDI CPRDFKAWFG LGQAYALLDM HLYSLYYFQK ACTLKPWDRR 500
IWQVLGECYS KTGNKVEAIK CYKRSIKASQ TVDQNTSIYY RLAQLYEELE 550
DLQECKKFMM KCVDVEELLE GIVTDETVKA RLWLAIFEIK AGNYQLAYDY 600
AMGVSSGTSQ EIEEARMLAR ECRRHMAAGR RIPGGHHHHH
```

Figure S6: Ni-NTA-Nanogold labeling of Apc11 and Cdc23.

(**A**) Electron micrograph of $APC^{Apc11\text{-}6His}$ labelled with Ni-NTA-Nanogold. Individual Nanogold labels were not clearly visible on the micrographs and only became apparent in class averages (Figure 6A). The large gold clusters seen on the micrographs are probably clusters of several Nanogold particles randomly distributed

on the grids. The scale bar is 100 nm. (**B,C**) Sequence of the (**B**) Apc11-6His and (**C**) Cdc23-6His proteins. The RING domain in Apc11 is highlighted in bold and zinc-chelating residues (red) were mapped by sequence alignment to Rbx1 (Zheng et al., 2002). The positions of eleven predicted TPR motifs in Cdc23 are shown in alternating shades of green. The C-terminal tags are shown in italics with the six histidine residues in blue.